Nanoscale

PAPER

View Article Online
View Journal

Cite this: DOI: 10.1039/d5nr05147a

Intrinsic electrocatalytic activity of nitrogen-doped monolayer graphene observed using a Janus bilayer design

Gloria Alexander, [a] Tobias Grosser,[a] Cathy Sulaiman, [b] Raquel Sánchez-Barquilla, [b] Emil Fuhry,[a] Isabell Wachta, [a] Robert Jungnickel,[a] Jan Ingo Flege [b] and Kannan Balasubramanian *[a]

Nitrogen doping is a widely-used strategy for enhancing the electronic and electrocatalytic properties of graphene. On single-sheet graphene electrodes, substrate-induced charge density effects obscure their intrinsic behavior and limit the efficiency of surface-sensitive electron transfer. Here, we report a Janus bilayer electrode architecture that decouples a nitrogen-doped graphene top layer from the substrate *via* a pristine graphene bottom layer. This design allows the presentation of catalytically active nitrogen sites while simultaneously suppressing substrate effects, enabling a direct evaluation of the intrinsic effect of nitrogen-doping on the electron transfer (ET) properties of graphene. Using ferricyanide as a redox-probe, we show that the ET kinetics of pristine bilayer graphene are pH-dependent, while nitrogen-doped bilayer graphene displays stable, pH-independent redox behavior. As an application avenue of biological relevance, we demonstrate that nitrogen-doped bilayer graphene exhibits a reduced overpotential for NADH oxidation. These results demonstrate that the synergy between substrate decoupling and controlled nitrogen incorporation yields a robust electrode architecture with enhanced stability and improved electrocatalytic activity.

Received 7th December 2025,
Accepted 20th February 2026

DOI: 10.1039/d5nr05147a

rsc.li/nanoscale

Introduction

Nitrogen doping[1–3] is a viable route for tuning the interfacial, electronic and electrochemical properties of chemical vapor deposition (CVD)-grown graphene[4,5] and chemically derived graphene.[6–9] Due to the abundance of catalytically active sites, electrodes based on nitrogen-doped graphene derivatives have been explored in a broad range of applications including electrocatalysis,[9,10] fuel-cells,[4] batteries,[11,12] supercapacitors,[13] and biosensors.[14,15] The incorporation of nitrogen, in the form of pyridinic, pyrrolic and graphitic N-functionalities, alters the chemical nature of the graphitic surface and enhances its electron transfer (ET) capability.[3,7,16] Specifically, pyridinic N refers to nitrogen atoms at the edge or defect sites bonded to two carbons. Pyrrolic N is incorporated into a five-membered ring, and graphitic N substitutes carbon within the basal plane while being bonded to three carbon atoms.[3,16]

N-doping of graphene derivatives has often been experimented in the context of the oxygen reduction reaction (ORR), for which the pyridinic N is considered a key component in achieving a low overpotential.[1,3] Pyrrolic N has also been shown to provide an improvement in electrocatalytic activity, albeit to a comparatively smaller extent.[3,8,16] In both cases, it has been proposed that carbon atoms adjacent to the *N*-substitution provide favorable oxygen adsorption sites facilitating the reduction.[3,16] On the other hand, graphitic nitrogen enhances the overall electronic conductivity and modulates the charge distribution, thereby supporting the catalytic effect.[4,8,17,18] Together, these nitrogen configurations enable a versatile control over both the local interfacial chemistry and the global electronic properties of graphitic structures in an electrode. The role of different nitrogen substitutions for other electrochemical reactions has not yet been investigated in detail.

In most of the previous experimental works, the intrinsic effect of N-doping has seldom been studied at an isolated single-sheet level. For this purpose, CVD-grown single-layer graphene (SLG) is ideally suited. The electrochemistry of SLG has been widely studied using canonical redox probes such as hexacyanoferrate(II/III) $[Fe(CN)_6^{3-/4-}]$ ($FeCN_6$).[19–21] The ET with $FeCN_6$ was often reported to be sluggish, which is partly attributed to the low electronic density of states (DOS) of pristine graphene.[19,22] Moreover, ET with $FeCN_6$ is generally sensitive

[a]*Department of Chemistry and School of Analytical Sciences Adlershof (SALSA), Humboldt-Universität zu Berlin, Germany. E-mail: nano.anchem@hu-berlin.de*
[b]*Chair of Applied Physics and Semiconductor Spectroscopy, Brandenburg University of Technology Cottbus-Senftenberg, 03046 Cottbus, Germany*

to the chemical nature of the graphene surface and hence is considered a surface-sensitive (SS) redox probe.[19,22,23] Since the first intermediate step in most electrocatalytic reactions involves a chemical interaction with the electrode surface, $FeCN_6$ serves as a good model redox probe to assess the electrocatalytic activity.[23]

Chemical modification of graphene either in the form of crystal doping or surface functionalization is a viable route to modulate the efficiency of SS-ET and to impart electrocatalytic properties. An unambiguous monitoring of SS-ET, when using single-layer graphene (SLG) as an electrode, remains challenging due to two reasons. First, the ET rates are considerably influenced by the substrate.[24,25] For instance, on metallic substrates, hybridization between the DOS of graphene and the subsurface metal was shown to enhance ET rates for $FeCN_6$, rendering graphene nearly electronically transparent.[26] Even on insulating substrates, surface ionizable groups (*e.g.* silanol groups on SiO_2/Si) influence the interfacial charge contribution modulating the reactivity.[27] Such substrate-induced charge density effects can obscure or distort the intrinsic behavior of nitrogen-doped graphene, making it challenging to clearly resolve the intrinsic contribution of nitrogen functionalities.

A second factor is the effective charge distribution at the graphene–liquid interface (GLI), which plays a significant role in modulating the ET kinetics through electrostatic effects.[28,29] The point of zero charge of unmodified graphene on SiO_2/Si is reported to be less than 3, rendering the graphene surface more negatively charged at higher pH.[28] With an anionic redox probe such as $FeCN_6$, it was demonstrated that the ET rate is pH-dependent and is one order of magnitude lower at pH 7 than at pH 3.[29] This effect was found to vary from one insulating substrate to another suggesting that charge density variations of the underlying insulating substrate additionally modulate the interfacial charge at the GLI thereby affecting the ET kinetics.[29] In contrast, on glassy carbon or on gold electrodes, there is negligible pH dependence of ET rates, confirming that this electrostatic effect is characteristic for supported graphene monolayers.[29] Another example is the variation in the ET rates of diazonium salts at SLG electrodes supported on different substrates.[27]

To address these two challenges simultaneously and deduce the intrinsic effect of N-doping, we devised a Janus bilayer electrode architecture to integrate nitrogen-based activation of the graphene surface with an effective suppression of the substrate effects. Janus 2D materials, where two sheets of a 2D material with asymmetric chemical nature are integrated in a bilayer, allow for extending the functional complexity with novel properties such as improved reactivity.[30–32] For example, Janus bilayer graphene with the top layer made hydrophilic for favorable biomolecule adsorption and an unmodified bottom layer as a robust support could be used efficiently as an electron microscopy grid.[33] Devices made of a Janus bilayer with an oxygen plasma treated top layer and a pristine bottom layer on an insulating substrate were shown to be promising for biosensing applications.[34–36] Until now, such Janus bilayer graphene has neither been used for studying electrocatalysis nor for minimizing substrate effects.

In our nitrogen-doped Janus bilayer graphene (N-BLG), a pristine graphene bottom layer minimizes substrate-induced charge density effects, whereas a nitrogen-doped top layer introduces catalytically active sites that selectively modulate the ET with SS redox species. This design shields the support material from the electrolyte while preserving a well-defined GLI for electrochemical reactions. Using this approach, we demonstrate that nitrogen doping of graphene enables a stable elimination of pH-dependent ET variations with enhanced kinetics. As an application, we present a clear improvement in electrocatalytic activity for the oxidation of NADH (nicotinamide adenine dinucleotide, reduced form) at the N-BLG compared to pristine bilayer graphene (BLG).

Results and discussion

For realizing N-doped graphene, several methods have been proposed such as direct introduction of ammonia during CVD growth,[4,5] heat treatment in ammonia post-growth,[1] and plasma treatment in nitrogen[7,37] or ammonia.[38] We utilized a gentle nitrogen plasma treatment to incorporate nitrogen into the graphene lattice. Fig. 1 presents a scheme of the preparation of N-BLG, which is based on a standard wet-transfer method.[29,39–41] CVD-grown graphene on copper foil was first coated with polystyrene and the underlying copper was removed using a metal-free etching solution. The SLG sheet with polystyrene was transferred onto a SiO_2/Si substrate with pre-patterned contacts, followed by dissolution of polystyrene. A second graphene sheet (on copper) is modified using a mild plasma treatment in nitrogen (6 s) and transferred on top of the pristine bottom layer to form the N-BLG electrode (see optical images in Fig. S1 in SI). After transfer, trace metal impurities were removed by electrochemical etching (Fig. S2 in SI).[42]

Fig. 2(a) presents an atomic force microscopy (AFM) height image of the pristine SLG on SiO_2/Si after transfer, while Fig. 2(b) shows the same location after subsequent transfer of a N-doped SLG (N-SLG) sheet. The presence of single layer graphene is confirmed from AFM section profiles (see Fig. S3 in SI). In Fig. 2(a), the first graphene layer is clearly visible, showing characteristic folds and wrinkles typical for transferred monolayers. After transfer of the top layer (Fig. 2(b)), the folds in the bottom layer are still intact and visible, indicating a uniform coverage. Moreover, the surface of N-BLG is more hydrophilic than the first layer as observed by contact angle measurements (Fig. S4, SI), confirming a successful transfer.

Confocal Raman spectroscopy was used to further verify the presence of the bilayer structure (Fig. 2c). SLG exhibits a negligible D peak intensity (at ~1350 cm^{-1}) and a sharp 2D peak (at ~2700 cm^{-1}), which is characteristic for SLG with a low defect density.[43–45] The relative intensities of the G and 2D peaks are comparable, which is typical for our SLG samples on SiO_2/Si.[39,40] Both for the pristine BLG (where both layers are unmodified) and for N-BLG, the 2D band is broader (see Fig. S5 in

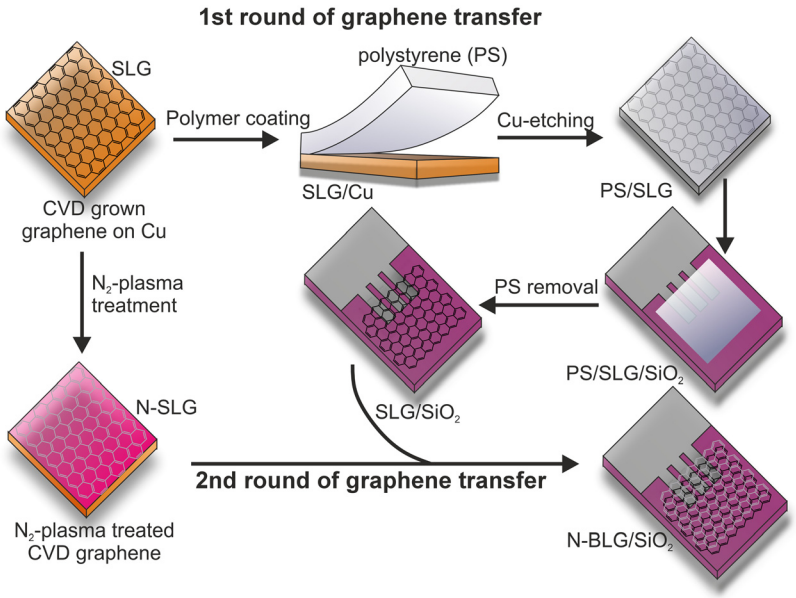

Fig. 1 Schematic illustration of the fabrication of a nitrogen-doped Janus bilayer graphene (N-BLG) electrode. (Top row) CVD-grown graphene on copper foil is first coated with polystyrene (PS) and the copper is removed by chemical etching. (Middle row) The PS/graphene stack is transferred onto a SiO_2/Si substrate followed by dissolution of PS. (Bottom row) A second CVD-grown graphene sheet is treated with a mild nitrogen plasma to incorporate nitrogen functionalities (N-SLG), then transferred on top of the pristine bottom layer (SLG) to complete the realization of the bilayer electrode (N-BLG).

SI) and blue shifted confirming the presence of a bilayer.[44] Its comparatively lower intensity with respect to the G peak additionally suggests the occurrence of a misoriented bilayer.[46] In the Raman spectrum of N-BLG, the D peak is prominent with a relatively higher intensity. Moreover, a subtle onset of the D′ shoulder is visible close to the G peak.[47] These two features are consistent with increased disorder typically expected from the plasma treatment due to nitrogen incorporation.[5,38,48]

X-ray photoelectron spectroscopy (XPS) is widely used to characterize nitrogen-doped graphene, since it provides direct information on the elemental composition of the sample near-surface region and the chemical bonding environment of the photo-excited atom, thus serving to identify the types of nitrogen functionalities introduced.[6,7] Fig. 3(a) presents a high-resolution carbon 1s XPS spectrum of N-doped graphene (on copper) prepared by nitrogen plasma treatment for 6 s. Based on previous XPS analysis,[29,39,49,50] the main peak around 284.5 eV is attributed to a dominant sp^2 carbon component with a small sp^3 contribution, indicating the presence of a largely intact graphene lattice. The peak at higher binding energy is assigned to the occurrence of C–N functionalities, confirming successful nitrogen incorporation.[7] Fig. 3(b) shows the nitrogen 1s XPS spectrum of the same sample. Based on previous works,[1,3,6] the different peaks can be assigned to pyridinic N (~61%), pyrrolic N (~36%) and graphitic N (~3%) moieties, as indicated in the Figure. A full survey spectrum is shown in Fig. S6 (SI). A direct comparison with the XPS data of pristine SLG is depicted in Fig. S7; further explanations regarding the fit model and the peak assignment are deferred to the SI. From the Raman spectrum, showing intact graphene-related peaks, and from the C 1s XPS spectrum, it can be inferred that the plasma conditions used here induce a rather low density of nitrogen sites, while largely preserving the graphene lattice. A higher density can be achieved by increasing the duration of plasma treatment, as discussed later. XPS measurements on the same sample after four days revealed a modest (~12%) decrease in pyridinic N component (Fig. S8 and Table S1, SI), suggesting some redistribution or gradual loss of pyridinic nitrogen species over time.

Now we turn towards the electrochemical behavior of N-BLG in comparison to that of pristine BLG. Fig. 4(a) and (b) present the cyclic voltammograms (CVs) of pristine BLG and N-BLG respectively using $FeCN_6$ as a redox probe in buffers of pH 3, 5, and 7. Despite the additional graphene layer for substrate shielding in pristine BLG, a prominent pH-dependent response is discernible (Fig. 4(a)), similar to the behavior reported for SLG (see Fig. S9 in SI) and discussed previously in the literature.[29] The black curve in Fig. 4(c) presents the evolution of peak-to-peak separation (ΔE_{pp}) as a function of pH for pristine BLG, where it is apparent that the peak spacing increases with increasing pH. This implies a faster ET at lower pH, consistent with electrostatic effects playing a dominant role in ET with the anionic $FeCN_6$ even on pristine BLG. In striking contrast, N-BLG exhibits rather constant redox-peak potentials and small and stable ΔE_{pp} across all pH values (blue curve in Fig. 4(c)), indicating a reversible ET and a complete elimination of pH dependence. CVs recorded with the cationic redox probe hexaammineruthenium(III) chloride $[Ru(NH_3)_6]^{3+}$ also displayed reversible ET behavior on N-BLG

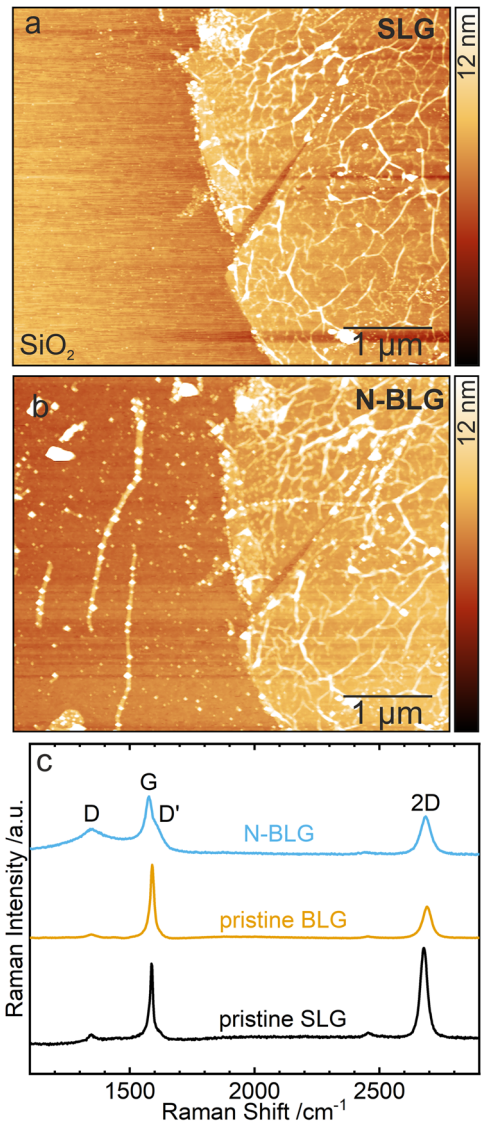

Fig. 2 (a and b) AFM height images of single-layer graphene (SLG) after the first transfer (a) and nitrogen-doped bilayer graphene (N-BLG) after the second transfer (b). (c) Confocal Raman spectra of SLG, pristine BLG and N-BLG. Excitation wavelength: 532 nm. In the pristine BLG, both the top and bottom layers are unmodified. Refer to Fig. S3 in SI for section profile of SLG.

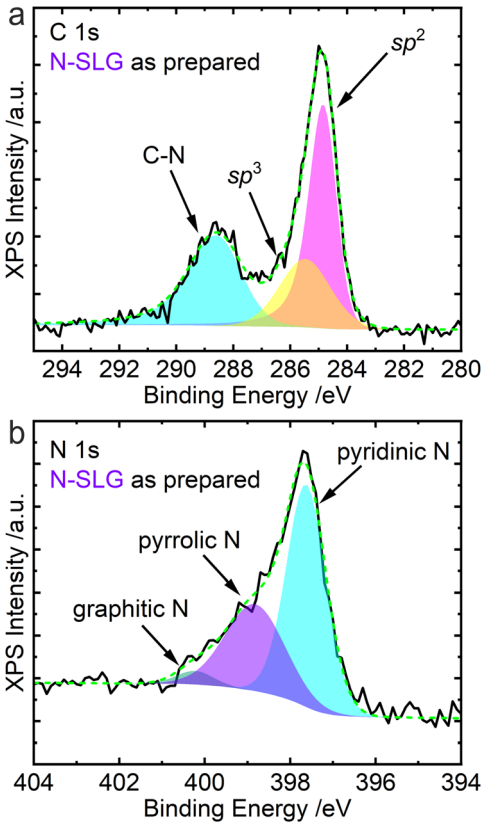

Fig. 3 XPS spectra of nitrogen-doped graphene (N-SLG) prepared by a gentle nitrogen plasma treatment for 6 s. (a) High resolution carbon 1s spectrum showing dominant sp^2 and minor sp^3 contributions with a strong C–N component, indicating an intact graphene lattice with successful nitrogen incorporation. (b) High resolution nitrogen 1s spectrum showing predominantly pyridinic nitrogen (~61%), followed by pyrrolic nitrogen (~36%) and minor graphitic nitrogen (~3%). A full survey spectrum is shown in Fig. S6 (SI). See Fig. S7 in SI for detailed XPS interpretation.

(see Fig. S10 in SI), indicating that the pH-independent response is not limited to anionic species but extends to cationic redox systems as well.

To highlight the importance of a bottom graphene layer, we have also investigated the electrochemistry of N-SLG deposited directly on the SiO_2/Si substrate. CVs measured immediately after preparation showed a suppression of pH-dependent shifts. However, this effect was found to be transient, as the pH dependence reappeared within two days (Fig. 5(a)). We attribute this instability to the continued influence of charged impurities in the underlying substrate that is in direct contact with the monolayer.[27] In contrast, N-BLG retained stable and pH-independent peak spacings even after one week under ambient storage (Fig. 5(b)). Here, the bottom graphene layer effectively screens the substrate effects and provides an electronically decoupled, stable support for the N-doped top layer.

These observations demonstrate that the Janus bilayer design uniquely combines substrate shielding together with nitrogen-based activation of the top layer, successfully mitigating electrostatic effects in SS-ET on graphene. Our data suggest that the presented approach was successful in inducing a similar interfacial charge density at the GLI across the investigated pH range of 3 to 7. We attribute this capability to the combination of pyridinic and pyrrolic groups in the N-doped top layer, which have significantly different pK_a values (pyridine: 4.7–5.1, pyrrole >17, graphitic N <–17).[51] Moreover, the low overall nitrogen density indicates that there is still a considerable amount of unmodified graphene regions on our electrodes. Thus, the coexistence of doped and undoped graphene regions, and the stabilizing contribution of the underlying pristine graphene layer, together create a balanced interfacial charge environment for ET. This synergistic configuration is

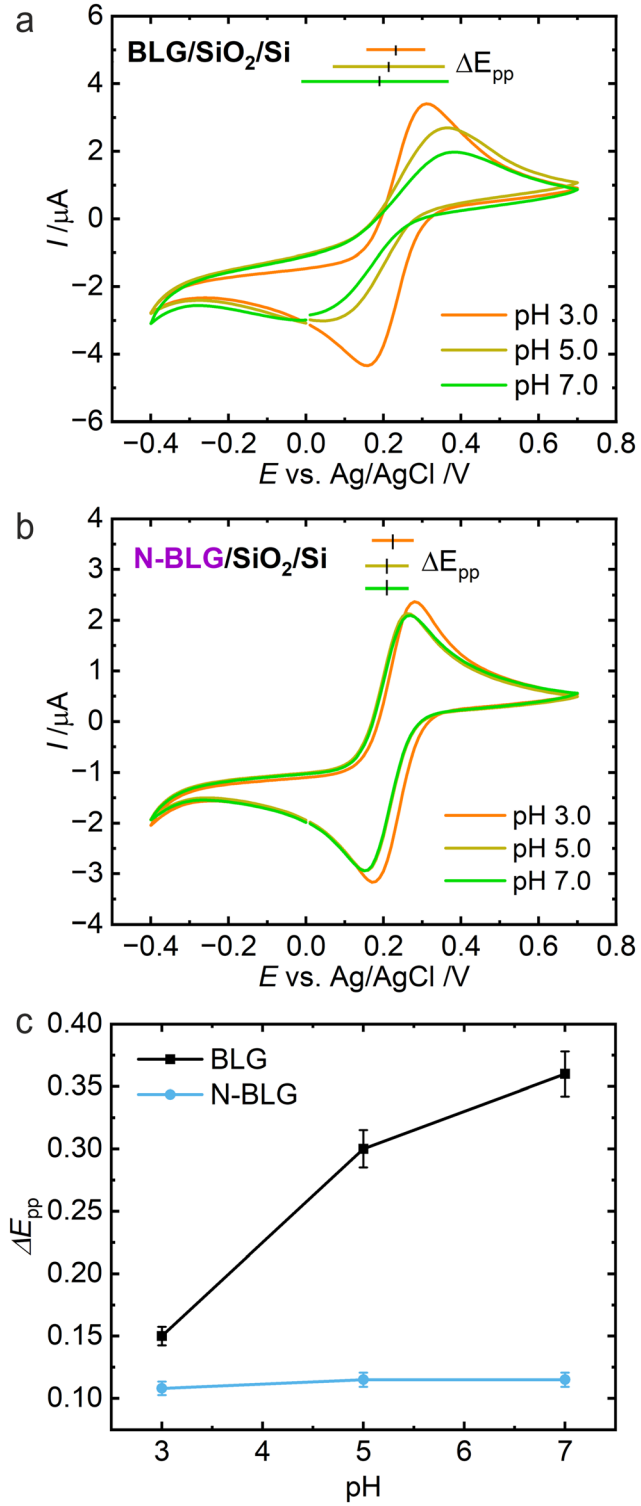

Fig. 4 (a and b) Cyclic voltammograms (CVs) of pristine BLG (a) and N-BLG (b) electrodes recorded in 1 mM $FeCN_6$ in buffers of pH 3, 5 and 7. Scan rate: 50 mV s^{-1}. (c) Peak-to-peak spacing (ΔE_{pp}) as a function of pH extracted from the CVs for the two electrodes.

key to achieving a stable, pH-independent ET for the SS redox probe $FeCN_6$. Further confirmation for the improved ET characteristics of N-BLG is obtained from electrochemical

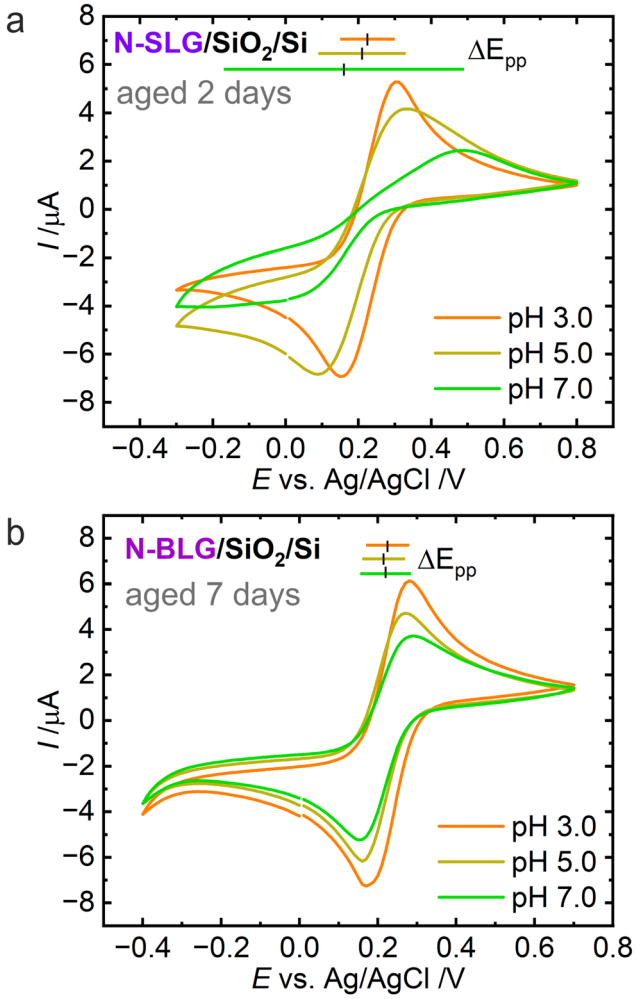

Fig. 5 Aging effect in N-SLG and N-BLG. (a and b) CVs of aged N-SLG (a) and aged N-BLG (b) electrodes recorded in 1 mM ferricyanide in buffers of pH 3, 5 and 7. Scan rate: 50 mV s^{-1}. In (a) the CV was measured two days after preparation, while in (b) the CV was measured one week after preparation. The samples were stored in ambient after preparation.

impedance spectroscopy (see Fig. S11 in SI). The charge transfer resistance for $FeCN_6$ at pH 7 was found to be at least an order of magnitude lower on N-BLG than on pristine BLG.

Apart from the three major N-modification types discussed above, there is the possibility of formation of pyridonic moieties from the pyridinic N end-groups.[3,25,52] In an XPS spectrum, the peak for the pyridonic functionality is very close to that of a pyrrolic moiety.[3] Such a transformation has however been observed after thermal treatment in oxygen[53] or after electrochemical cycling in ORR.[25,52] Moreover, they require a high density of edges.[25] Since we do not have these conditions in our experiments, we exclude the introduction of such functional groups through our plasma treatment. Even if such groups were present on our N-doped graphene, the observed pH-independent ET kinetics confirm that they contribute favorably to the establishment of a balanced charge landscape.

We next exploited the enhanced catalytic effect of our N-BLG electrodes for the investigation of NADH, a biologically relevant redox probe, whose oxidation is known to be surface-sensitive with a high overpotential at carbon-based electrodes.[54–56] N-doping of carbon electrodes is known to favor the oxidation of NADH by decreasing the overpotential and increasing the current density. However, until now, this effect has been demonstrated only on electrodes based on reduced graphene oxide (RGO).[14,15,57] N-doped CVD-grown graphene has not yet been used for studying the redox behavior of NADH.

Fig. 6(a) presents the CVs of NADH at pristine BLG and N-BLG. Compared to pristine BLG, N-BLG prepared by a 6 s plasma treatment exhibits a remarkably lower overpotential with a downshift of ~160 mV, signifying improved ET kinetics. Similar low overpotentials have been reported for N-doped RGO.[15] In these electrodes, residual functionalities remaining from chemical processing may be redox active and act as mediators for NADH oxidation.[14] In our case, the absence of any redox-active peaks in the blank CVs (see Fig. S12 in SI) indicates that the reduction in overpotential originates intrinsically from N-doping of the graphene surface. Thus, our findings support earlier observations on N-doped RGO and provide direct evidence that controlled N-doping itself is sufficient to enhance the electrocatalytic oxidation of NADH. The realized N-BLG electrodes were found to be stable under continuous cycling in NADH (see Fig. S13 in SI).

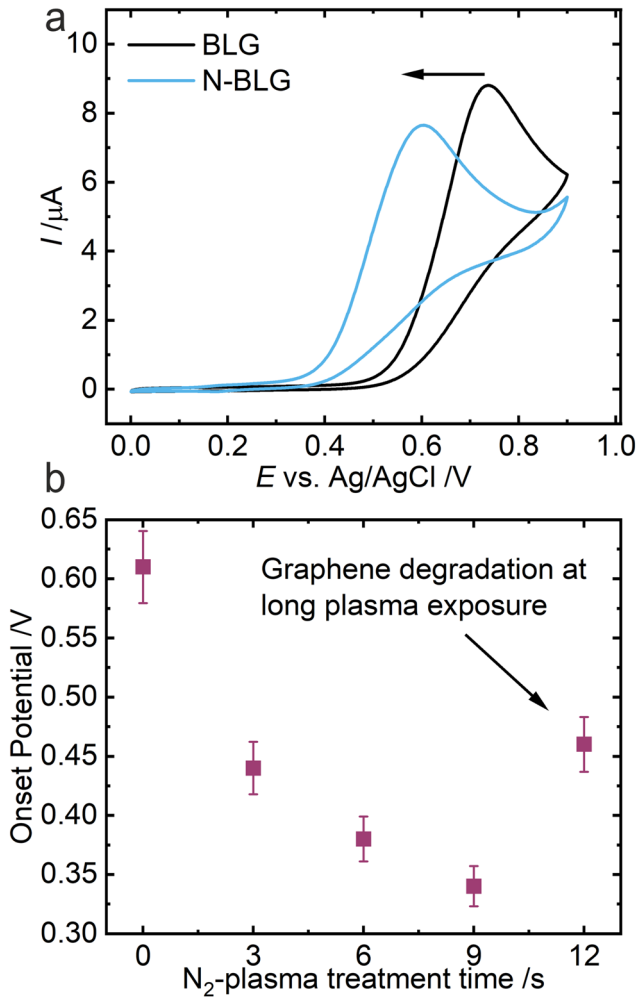

Fig. 6 (a) CVs of NADH oxidation at pristine BLG and N-BLG electrodes. N-BLG exhibits a reduced onset potential (~160 mV shift) compared to BLG, as indicated by the arrow. (b) Onset potential for NADH oxidation as a function of the duration of nitrogen plasma treatment. The lowest onset potential is observed for intermediate plasma exposures (6–9 s), while excessive plasma treatment (>12 s) results in an increase in onset potential.

To evaluate the tunability of nitrogen incorporation and its effect on the redox behavior, the plasma treatment duration was varied and the overpotential for NADH oxidation extracted (see Fig. 6(b)). Optimal electrocatalytic performance was observed for intermediate plasma exposures (6–9 s), while excessive plasma treatment (>12 s) was found to cause damage to the graphene sheet, yielding a higher overpotential for NADH oxidation (see Fig. S14 in SI). These observations establish N-BLG as a tunable and efficient electrode material for NADH oxidation.

It is worth mentioning that we have also evaluated the possibility of using our N-BLG electrode for ORR (see Fig. S15 in SI). However, compared to pristine BLG, we observed only a slight improvement in the electrocatalytic activity under acidic conditions. This can be understood by considering that our N-BLG electrodes have a combination of pyridinic and pyrrolic N. As mentioned in the introduction, pyridinic N is considered to be essential to bring about a significant improvement in electrocatalytic activity for ORR.[1,17] Pyrrolic N has also been suggested as an electrocatalytic site for ORR,[4] however, the improvement in overpotential is not as substantial as in electrodes with predominant pyridinic-N.[8] Since we do not have exclusively pyridinic nitrogen, the electrocatalysis is not optimal for ORR. On the other hand, our results show that a combination of pyridinic and pyrrolic N is well-suited for reducing the overpotential for biological redox reactions (*e.g.*, NADH oxidation) as well as for minimizing the electrostatic effects on ET kinetics.

Conclusion

In summary, we have shown that the pH-dependence of the electrochemical response of SS redox species at graphene could be successfully mitigated by combining nitrogen doping with our Janus bilayer architecture. The pristine bottom layer effectively minimizes substrate-induced charge density effects, by decoupling the active graphene surface from the substrate. At the same time, nitrogen doping of the top layer introduces a balanced charge density landscape that suppresses pH-dependent electrostatic influence at the GLI, enhances ET kinetics and significantly reduces the overpotential for NADH oxidation. The synergy between substrate decoupling and controlled, low-density nitrogen doping is crucial for achieving the observed stability and performance. In general, a Janus bilayer

architecture provides a versatile avenue for decoupling substrate effects on the electrochemistry of 2D materials. In the future, this approach can be exploited for systematic investigations of electrocatalyst materials on graphene in their intrinsic form.

Experimental

Chemicals

All solutions were prepared with ultra-pure water (Barnstead Easypure II, 18.2 MΩ cm^{-1}). Hydrochloric acid (37 wt%, p.a., Emsure), polystyrene (PS, av. M_w 35 000), toluene (≥ 99.8%, Rotisolv), potassium hexacyanoferrate(III) (ferricyanide, 99.98% trace metal basis), β-nicotinamide adenine dinucleotide (NADH, reduced disodium salt), hexammineruthenium(III) chloride (HARu, 98%) and perchloric acid (70 wt%, ACS reagent) were purchased from Sigma-Aldrich. 1,1′-Ferrocenedimethanol (FDM, 98.11%) was purchased from BLD Pharm. Hydrogen peroxide (30%, Ph.Eur. stabilized) and *N*-methyl-2-pyrrolidone (≥99.8%) were purchased from Roth. Acetone and isopropanol were purchased in VLSI Selectipur quality from BASF. CVD-grown graphene on copper foil was purchased from Graphenea Inc.

Substrate preparation and cleaning

Ti/Pt (50 nm/10 nm) electrode lines were prepared by photolithography followed by metal deposition on SiO_2/Si (thickness 500 nm). The silicon wafers were cleaned in *N*-methyl-2-pyrrolidone (NMP), acetone and isopropanol with ultrasonication at 40 °C. An RCA cleaning method was then applied: the wafers were ultrasonicated first in an oxidizing base (10 : 1 : 1 v/v/v $H_2O : H_2O_2 : NH_3$), followed by an oxidizing acid (10 : 1 : 1 v/v/v $H_2O : H_2O_2 : HCl$). Finally, the wafers were cleaned with O_2-plasma for 5 minutes.

Nitrogen-doping by N_2-plasma

Nitrogen doping of CVD graphene was performed using a Diener Electronic plasma system (Femto-ARS-c; 40 kHz, maximum power 100 W) operated with N_2 gas at a power of 50 W. CVD graphene grown on Cu was introduced directly into the chamber, and each sample was treated for 6 s, unless stated otherwise. Afterwards, a standard wet transfer was carried out.

CVD graphene transfer

CVD-grown graphene on Cu was cut into rectangular pieces (a few mm^2 in size) and a polystyrene (PS) solution (50 mg mL^{-1} in toluene) was drop-cast onto the pieces. The PS/Gr/Cu stack was dried at 75 °C for 15 minutes. A standard metal-free wet transfer was then performed using an etching solution (60 : 6 : 1 v/v/v $H_2O : HCl$ (37%) : H_2O_2 (30%)) to remove the underlying Cu foil. The PS-coated graphene was transferred onto the patterned SiO_2/Si wafers and dried for 20 minutes. PS was then removed by immersing the samples in a toluene bath for 5 minutes, followed by gentle blow-drying. The chips were annealed at 500 °C under nitrogen atmosphere for 10 minutes. The second graphene layer was applied in the same way. To avoid parasitic electrochemical/electrocatalytic activity, we use electrochemical etching to remove trace metal ions from transferred graphene.[42] This etching was performed in 100 mM HCl with 20 scans over a potential range of −0.6 to +0.4 V *vs.* Ag/AgCl at a scan rate of 50 mV s^{-1}.

Surface characterization

A Bruker JPK Nanowizard 4 atomic force microscope (AFM) was used for surface imaging. AFM images were processed using Gwyddion. The Raman spectra of graphene on SiO_2/Si were obtained using a JASCO NRS-4100 Raman spectrometer equipped with a 1650 × 256 CCD detector (Andor, air/Peltier-cooled to −60 °C), a 900 L mm^{-1} grating, a 532 nm diode laser and a 100× (NA 0.90) objective. The laser power was maintained at 5.6 mW for all acquisitions. Each Raman spectrum was recorded with an exposure time of 3 s and 5 accumulations. The instrument was calibrated before data acquisition using the Si substrate peak at 520.7 cm^{-1}. Raman spectra were processed using Origin 2024; the baseline was corrected using a spline-fit baseline and normalized to the G-peak intensity.

X-ray photoelectron spectroscopy (XPS)

Soft XPS measurements were performed using a monochromatized Al K_α X-ray source (XR 50 M), and Phoibos 150 hemispherical energy analyzer from SPECS. The pass energy was set to 50 eV for the survey and 20 eV for the detailed scans of the specific regions. These values yield spectral resolutions of 1.1 eV and 0.6 eV, respectively. Sample charging was corrected using the Cu $2p_{3/2}$ peak at 933 eV as a reference.[58] Data were processed and decomposed using the CasaXPS software, version 2.3.18PR1.0. A Shirley background was applied to all spectra, and peak fitting was carried out using a symmetric Gaussian–Lorentzian (GL) line shape for all the peaks and the CN and sp^2 carbon peaks were fit with an asymmetric line-shape function (LA). The full width at half maximum (FWHM) and GL/LA ratio were fixed for each component.

Electrochemical setup and measurement

Electrochemical measurements with the graphene electrodes (N-BLG, BLG and N-SLG) as working electrodes were performed in a standard three-electrode configuration using an Ivium CompactStat potentiostat. A Pt wire served as the counter electrode and a commercial Ag/AgCl (3 M KCl) electrode as the reference electrode. Measurements were carried out in phosphate buffer (pH 3.0 and 7.0) and acetate buffer (pH 5.0) using a concentration of 10 mM with 0.1 M KCl as supporting electrolyte. Cyclic voltammetry (CV) was performed at a scan rate of 50 mV s^{-1}. The redox probe concentrations were 1 mM for ferricyanide and 10 μM for NADH. Oxygen reduction reaction (ORR) measurements were performed in 100 mM $HClO_4$. The solutions were bubbled with oxygen or nitrogen (as indicated in the graphs) at least for half an hour prior to the measurements.

Contact angle measurements

A custom-built contact angle measurement system was used to measure the water contact angles of the Si/SiO_2 samples. The setup consisted of a light source (ORLEGOL, VL49RGB), a Z-translation stage (Rotilabo®), a precision pipette (Eppendorf Research plus) and a camera system (IDCP B.V., Dino-Lite, AM73915MZTL). For each measurement, a 1 μL droplet of deionized water was placed on the surface of the material using the precision pipette and an image of the droplet was recorded. Images were processed in ImageJ using the contact angle plugin. All measurements were repeated at least three times to ensure accuracy and reproducibility. Experiments were performed under standard atmospheric conditions without temperature control.

Author contributions

Gloria Alexander: investigation, methodology, data curation, writing – original draft, writing – review and editing; Tobias Grosser: methodology, writing – review and editing; Cathy Sulaiman: investigation, data curation, writing – original draft, writing – review and editing; Raquel Sánchez-Barquilla: investigation, data curation, writing – original draft, writing – review and editing; Emil Fuhry: investigation, data curation, writing – review and editing; Isabell Wachta: writing – review and editing; Robert Jungnickel: writing – review and editing; Jan Ingo Flege: resources, supervision, writing – review and editing; Kannan Balasubramanian: methodology, resources, conceptualization, supervision, writing – original draft, writing – review and editing.

Conflicts of interest

The authors declare no conflicts of interest.

Data availability

The data supporting the conclusions of this article are included in the article and as part of supplementary information (SI). Supplementary information includes optical microscopy images of the graphene coverage, AFM height profile section, water contact angle measurements, Raman spectroscopy data, XPS analysis of pristine SLG and N-SLG (aging studies), electrochemical impedance spectroscopy (EIS) with equivalent circuit fitting and extracted parameters, stability tests under prolonged NADH cycling, and additional electrochemical control experiments. See DOI: https://doi.org/10.1039/d5nr05147a.

Acknowledgements

We thank Isabelle Giehler and Julius Nürnberger of HU Berlin for their assistance with sample and buffer preparation.

References

1 D. Guo, R. Shibuya, C. Akiba, S. Saji, T. Kondo and J. Nakamura, Active sites of nitrogen-doped carbon materials for oxygen reduction reaction clarified using model catalysts, *Science*, 2016, **351**, 361–365.
2 Y. Jia, L. Zhang, L. Zhuang, H. Liu, X. Yan, X. Wang, J. Liu, J. Wang, Y. Zheng, Z. Xiao, E. Taran, J. Chen, D. Yang, Z. Zhu, S. Wang, L. Dai and X. Yao, Identification of active sites for acidic oxygen reduction on carbon catalysts with and without nitrogen doping, *Nat. Catal.*, 2019, **2**, 688–695.
3 J. Quílez-Bermejo, E. Morallón and D. Cazorla-Amorós, Metal-free heteroatom-doped carbon-based catalysts for ORR: A critical assessment about the role of heteroatoms, *Carbon*, 2020, **165**, 434–454.
4 L. Qu, Y. Liu, J.-B. Baek and L. Dai, Nitrogen-Doped Graphene as Efficient Metal-Free Electrocatalyst for Oxygen Reduction in Fuel Cells, *ACS Nano*, 2010, **4**, 1321–1326.
5 Z. Zafar, Z. H. Ni, X. Wu, Z. X. Shi, H. Y. Nan, J. Bai and L. T. Sun, Evolution of Raman spectra in nitrogen doped graphene, *Carbon*, 2013, **61**, 57–62.
6 M. K. Rabchinskii, S. D. Saveliev, D. Y. Stolyarova, M. Brzhezinskaya, D. A. Kirilenko, M. V. Baidakova, S. A. Ryzhkov, V. V. Shnitov, V. V. Sysoev and P. N. Brunkov, Modulating nitrogen species via N-doping and post annealing of graphene derivatives: XPS and XAS examination, *Carbon*, 2021, **182**, 593–604.
7 Y. Wang, Y. Shao, D. W. Matson, J. Li and Y. Lin, Nitrogen-doped graphene and its application in electrochemical biosensing, *ACS Nano*, 2010, **4**, 1790–1798.
8 L. F. Lai, J. R. Potts, D. Zhan, L. Wang, C. K. Poh, C. H. Tang, H. Gong, Z. X. Shen, L. Y. Jianyi and R. S. Ruoff, Exploration of the active center structure of nitrogen-doped graphene-based catalysts for oxygen reduction reaction, *Energy Environ. Sci.*, 2012, **5**, 7936–7942.
9 K. Parvez, S. Yang, Y. Hernandez, A. Winter, A. Turchanin, X. Feng and K. Mullen, Nitrogen-doped graphene and its iron-based composite as efficient electrocatalysts for oxygen reduction reaction, *ACS Nano*, 2012, **6**, 9541–9550.
10 R. Saini, F. Naaz, A. H. Bashal, A. H. Pandit and U. Farooq, Recent advances in nitrogen-doped graphene-based heterostructures and composites: mechanism and active sites for electrochemical ORR and HER, *Green Chem.*, 2024, **26**, 57–102.
11 K. Share, A. P. Cohn, R. Carter, B. Rogers and C. L. Pint, Role of Nitrogen-Doped Graphene for Improved High-Capacity Potassium Ion Battery Anodes, *ACS Nano*, 2016, **10**, 9738–9744.
12 V. R. Jauja-Ccana, L. La-Torre-Riveros, A. Cordova-Huaman, G. Huayta, L. Manfredy, A. Naupa, M. Isaacs and A. La Rosa-Toro, Review—Rational Design of Nitrogen-doped Graphene as Anode Material for Lithium-ion Batteries, *J. Electrochem. Soc.*, 2023, **170**, 040525.
13 E. Paek, A. J. Pak, K. E. Kweon and G. S. Hwang, On the Origin of the Enhanced Supercapacitor Performance of Nitrogen-Doped Graphene, *J. Phys. Chem. C*, 2013, **117**, 5610–5616.

14 P. P. Gai, C. E. Zhao, Y. Wang, E. S. Abdel-Halim, J. R. Zhang and J. J. Zhu, NADH dehydrogenase-like behavior of nitrogen-doped graphene and its application in NAD (+)-dependent dehydrogenase biosensing, *Biosens. Bioelectron.*, 2014, **62**, 170–176.
15 S. Mutyala and J. Mathiyarasu, A highly sensitive NADH biosensor using nitrogen doped graphene modified electrodes, *J. Electroanal. Chem.*, 2016, **775**, 329–336.
16 J. Liu, P. Song and W. Xu, Structure-activity relationship of doped-nitrogen (N)-based metal-free active sites on carbon for oxygen reduction reaction, *Carbon*, 2017, **115**, 763–772.
17 Q. Lv, W. Si, J. He, L. Sun, C. Zhang, N. Wang, Z. Yang, X. Li, X. Wang, W. Deng, Y. Long, C. Huang and Y. Li, Selectively nitrogen-doped carbon materials as superior metal-free catalysts for oxygen reduction, *Nat. Commun.*, 2018, **9**, 3376.
18 X. Ning, Y. Li, J. Ming, Q. Wang, H. Wang, Y. Cao, F. Peng, Y. Yang and H. Yu, Electronic synergism of pyridinic- and graphitic-nitrogen on N-doped carbons for the oxygen reduction reaction, *Chem. Sci.*, 2019, **10**, 1589–1596.
19 L. J. A. Macedo, R. M. Iost, A. Hassan, K. Balasubramanian and F. N. Crespilho, Bioelectronics and Interfaces Using Monolayer Graphene, *ChemElectroChem*, 2018, **6**, 31–59.
20 A. Ambrosi, C. K. Chua, N. M. Latiff, A. H. Loo, C. H. A. Wong, A. Y. S. Eng, A. Bonanni and M. Pumera, Graphene and its electrochemistry – an update, *Chem. Soc. Rev.*, 2016, **45**, 2458–2493.
21 M. Velický, D. F. Bradley, A. J. Cooper, E. W. Hill, I. A. Kinloch, A. Mishchenko, K. S. Novoselov, H. V. Patten, P. S. Toth, A. T. Valota, S. D. Worrall and R. A. W. Dryfe, Electron Transfer Kinetics on Mono- and Multilayer Graphene, *ACS Nano*, 2014, **8**, 10089–10100.
22 D. A. C. Brownson, S. A. Varey, F. Hussain, S. J. Haigh and C. E. Banks, Electrochemical properties of CVD grown pristine graphene: monolayer- vs. quasi-graphene, *Nanoscale*, 2014, **6**, 1607–1621.
23 J. F. Cassidy, R. C. de Carvalho and A. J. Betts, Use of Inner/Outer Sphere Terminology in Electrochemistry—A Hexacyanoferrate II/III Case Study, *Electrochemistry*, 2023, **4**, 313–349.
24 J. S. Hui, X. Zhou, R. Bhargava, A. Chinderle, J. R. Zhang and J. Rodríguez-López, Kinetic Modulation of Outer-Sphere Electron Transfer Reactions on Graphene Electrode with a Sub-surface Metal Substrate, *Electrochim. Acta*, 2016, **211**, 1016–1023.
25 N. Guo, K. M. Yam and C. Zhang, Substrate engineering of graphene reactivity: towards high-performance graphene-based catalysts, *npj 2D Mater. Appl.*, 2018, **2**, 1.
26 T. Bertaglia, T. J. Neubert, R. M. Iost, K. Balasubramanian and F. N. Crespilho, Consequences of edge and substrate modifications on graphene electrochemistry, *Curr. Opin. Electrochem.*, 2025, **50**, 101641.
27 Q. H. Wang, Z. Jin, K. K. Kim, A. J. Hilmer, G. L. Paulus, C. J. Shih, M. H. Ham, J. D. Sanchez-Yamagishi, K. Watanabe, T. Taniguchi, J. Kong, P. Jarillo-Herrero and M. S. Strano, Understanding and controlling the substrate effect on graphene electron-transfer chemistry via reactivity imprint lithography, *Nat. Chem.*, 2012, **4**, 724–732.
28 L. Zuccaro, J. Krieg, A. Desideri, K. Kern and K. Balasubramanian, Tuning the isoelectric point of graphene by electrochemical functionalization, *Sci. Rep.*, 2015, **5**, 11794.
29 M. Wehrhold, T. J. Neubert, A. Yadav, M. Vondracek, R. M. Iost, J. Honolka and K. Balasubramanian, pH sensitivity of interfacial electron transfer at a supported graphene monolayer, *Nanoscale*, 2019, **11**, 14742–14756.
30 V. Montes-García and P. Samorì, Janus 2D materials via asymmetric molecular functionalization, *Chem. Sci.*, 2022, **13**, 315–328.
31 L. Zhang, J. Yu, M. Yang, Q. Xie, H. Peng and Z. Liu, Janus graphene from asymmetric two-dimensional chemistry, *Nat. Commun.*, 2013, **4**, 1443.
32 M. A. Bissett, Y. Takesaki, M. Tsuji and H. Ago, Increased chemical reactivity achieved by asymmetrical 'Janus' functionalisation of graphene, *RSC Adv.*, 2014, **4**, 52215–52219.
33 L. Zheng, N. Liu, Y. Liu, N. Li, J. Zhang, C. Wang, W. Zhu, Y. Chen, D. Ying, J. Xu, Z. Yang, X. Gao, J. Tang, X. Wang, Z. Liang, R. Zou, Y. Li, P. Gao, X. Wei, H.-W. Wang and H. Peng, Atomically Thin Bilayer Janus Membranes for Cryo-electron Microscopy, *ACS Nano*, 2021, **15**, 16562–16571.
34 C.-H. Huang, T.-T. Huang, C.-H. Chiang, W.-T. Huang and Y.-T. Lin, A chemiresistive biosensor based on a layered graphene oxide/graphene composite for the sensitive and selective detection of circulating miRNA-21, *Biosens. Bioelectron.*, 2020, **164**, 112320.
35 C.-H. Huang, W.-T. Huang, T.-T. Huang, S.-H. Ciou, C.-F. Kuo, A.-H. Hsieh, Y.-S. Hsiao and Y.-J. Lee, Dual-Gate Enhancement of the Sensitivity of miRNA Detection of a Solution-Gated Field-Effect Transistor Featuring a Graphene Oxide/Graphene Layered Structure, *ACS Appl. Electron. Mater.*, 2021, **3**, 4300–4307.
36 S.-H. Ciou, A.-H. Hsieh, Y.-X. Lin, J.-L. Sei, M. Govindasamy, C.-F. Kuo and C.-H. Huang, Sensitive label-free detection of the biomarker phosphorylated tau-217 protein in Alzheimer's disease using a graphene-based solution-gated field effect transistor, *Biosens. Bioelectron.*, 2023, **228**, 115174.
37 M.-H. Tsai, C.-H. Lin, W.-T. Chen, C.-H. Huang, W.-Y. Woon and C.-T. Lin, Temperature Effect of Low-Damage Plasma for Nitrogen-Modification of Graphene, *ECS J. Solid State Sci. Technol.*, 2020, **9**, 121007.
38 M. Rybin, A. Pereyaslavtsev, T. Vasilieva, V. Myasnikov, I. Sokolov, A. Pavlova, E. Obraztsova, A. Khomich, V. Ralchenko and E. Obraztsova, Efficient nitrogen doping of graphene by plasma treatment, *Carbon*, 2016, **96**, 196–202.
39 M. Wehrhold, T. J. Neubert, T. Grosser, M. Vondracek, J. Honolka and K. Balasubramanian, A highly durable graphene monolayer electrode under long-term hydrogen evolution cycling, *Chem. Commun.*, 2022, **58**, 3823–3826.

40 T. J. Neubert, J. Krieg, A. Yadav and K. Balasubramanian, pH Sensitivity of Edge-Gated Graphene Field-Effect Devices with Covalent Edge Functionalization, *ACS Appl. Electron. Mater.*, 2022, **4**, 4668–4676.
41 V. Guglielmotti, E. Fuhry, T. J. Neubert, M. Kuhl, D. Pallarola and K. Balasubramanian, Real-Time Monitoring of Cell Adhesion onto a Soft Substrate by a Graphene Impedance Biosensor, *ACS Sens.*, 2024, **9**, 101–109.
42 R. M. Iost, F. N. Crespilho, L. Zuccaro, H. K. Yu, A. M. Wodtke, K. Kern and K. Balasubramanian, Enhancing the Electrochemical and Electronic Performance of CVD–Grown Graphene by Minimizing Trace Metal Impurities, *ChemElectroChem*, 2014, **1**, 2070–2074.
43 L. G. Cançado, A. Jorio, E. H. M. Ferreira, F. Stavale, C. A. Achete, R. B. Capaz, M. V. O. Moutinho, A. Lombardo, T. S. Kulmala and A. C. Ferrari, Quantifying Defects in Graphene via Raman Spectroscopy at Different Excitation Energies, *Nano Lett.*, 2011, **11**, 3190–3196.
44 A. C. Ferrari, J. C. Meyer, V. Scardaci, C. Casiraghi, M. Lazzeri, F. Mauri, S. Piscanec, D. Jiang, K. S. Novoselov, S. Roth and A. K. Geim, Raman Spectrum of Graphene and Graphene Layers, *Phys. Rev. Lett.*, 2006, **97**, 187401.
45 L. M. Malard, M. A. Pimenta, G. Dresselhaus and M. S. Dresselhaus, Raman spectroscopy in graphene, *Phys. Rep.*, 2009, **473**, 51–87.
46 K. Kim, S. Coh, L. Z. Tan, W. Regan, J. M. Yuk, E. Chatterjee, M. F. Crommie, M. L. Cohen, S. G. Louie and A. Zettl, Raman Spectroscopy Study of Rotated Double-Layer Graphene: Misorientation-Angle Dependence of Electronic Structure, *Phys. Rev. Lett.*, 2012, **108**, 246103.
47 A. Eckmann, A. Felten, A. Mishchenko, L. Britnell, R. Krupke, K. S. Novoselov and C. Casiraghi, Probing the Nature of Defects in Graphene by Raman Spectroscopy, *Nano Lett.*, 2012, **12**, 3925–3930.
48 G. Robert Bigras, X. Glad, P. Vinchon, R. Martel and L. Stafford, Selective nitrogen doping of graphene due to preferential healing of plasma-generated defects near grain boundaries, *npj 2D Mater. Appl.*, 2020, **4**, 42.
49 M. J. Webb, P. Palmgren, P. Pal, O. Karis and H. Grennberg, A simple method to produce almost perfect graphene on highly oriented pyrolytic graphite, *Carbon*, 2011, **49**, 3242–3249.
50 C. Morales, F. J. Urbanos, A. del Campo, D. Leinen, D. Granados, P. Prieto, L. Aballe, M. Foerster and L. Soriano, Influence of chemical and electronic inhomogeneities of graphene/copper on the growth of oxide thin films: the ZnO/graphene/copper case, *Nanotechnol.*, 2021, **32**, 245301.
51 B. Li, X. Sun and D. Su, Calibration of the basic strength of the nitrogen groups on the nanostructured carbon materials, *Phys. Chem. Chem. Phys.*, 2015, **17**, 6691–6694.
52 T. Xing, Y. Zheng, L. H. Li, B. C. Cowie, D. Gunzelmann, S. Z. Qiao, S. Huang and Y. Chen, Observation of active sites for oxygen reduction reaction on nitrogen-doped multilayer graphene, *ACS Nano*, 2014, **8**, 6856–6862.
53 A. Kumar, A. Ganguly and P. Papakonstantinou, Thermal stability study of nitrogen functionalities in a graphene network, *J. Phys.: Condens. Matter*, 2012, **24**, 235503.
54 J. Chen, J. C. Bao, C. X. Cai and T. H. Lu, Electrocatalytic oxidation of NADH at an ordered carbon nanotubes modified glassy carbon electrode, *Anal. Chim. Acta*, 2004, **516**, 29–34.
55 L. Blandón-Naranjo, J. Hoyos-Arbeláez, M. V. Vázquez, F. Della Pelle and D. Compagnone, NADH Oxidation onto Different Carbon-Based Sensors: Effect of Structure and Surface-Oxygenated Groups, *J. Sens.*, 2018, 6525919.
56 C. P. You, Y. Xuewu, Y. Wang, S. Zhang, J. Kong, D. Y. Zhao and B. H. Liu, Electrocatalytic oxidation of NADH based on bicontinuous gyroidal mesoporous carbon with low overpotential, *Electrochem. Commun.*, 2009, **11**, 227–230.
57 K. P. Prathish, M. M. Barsan, D. S. Geng, X. L. Sun and C. M. A. Brett, Chemically modified graphene and nitrogen-doped graphene: Electrochemical characterisation and sensing applications, *Electrochim. Acta*, 2013, **114**, 533–542.
58 J. F. Moulder, W. F. Stickle, P. E. Sobol and K. D. Bomben, *Handbook of X-ray Photoelectron Spectroscopy*, PerkinElmer Corporation, 1992.